Ninth International Conference on CFD in the Minerals and Process Industries
CSIRO, Melbourne, Australia
10-12 December 2012

METHODOLODGY FOR CFD-DEM MODELLING OF PARTICULATE SUSPENSION RHEOLOGY

Evan M. SMUTS[1*], Dave A. DEGLON[1] and Chris J. MEYER[2]

[1] Minerals to Metals, Department of Chemical Engineering, University of Cape Town, Cape Town 7701, SOUTH AFRICA

[2] Department of Mechanical and Mechatronic Engineering, Stellenbosch University, Stellenbosch 7602, SOUTH AFRICA

*Corresponding author, E-mail address: evan.smuts@gmail.com

ABSTRACT

This paper describes a methodology used to develop a numerical model for the study of particulate suspension rheology. Initially, Computational Fluid Dynamics (CFD) models of different rheometer geometries were tested with both a Newtonian fluid (water), and a non-Newtonian Herschel-Bulkley slurry. Rheograms were reproduced from these models and compared to experimental values. Once a single-phase model had been validated, a coupled model combining CFD and the Discrete Element Method (DEM) was created. Two open source software packages were chosen. CFD is implemented using OpenFOAM®, and DEM using LIGGGHTS. These two different codes were coupled via another programme called CFDEM. This coupled model is currently capable of modelling spherical particles in a suspending liquid. DLVO forces have been included in some models to account for inter-particle forces due to the surface charge on the particles. The coupled model is currently being validated. Preliminary results show good qualitative behaviour of the model.

NOMENCLATURE

A_H	Hamaker constant, J
c_{do}	drag coefficient, dimensionless
E	interaction energy, J
F	force, N
g	gravitational acceleration, m.s^{-2}
G	shear modulus, Pa
I	rotational inertia of particle, kg.m^2
k	elastic contact constant, kg.s^{-2}
K	fluid consistency index, Pa.s^n
m	particle mass, kg
M	particle torque, Nm
n	flow behaviour index, dimensionless
p	pressure, Pa
r	particle radius, m
r_c	cut-off distance, m
t	time, s
u	fluid velocity, m.s^{-1}
v	particle translational velocity, m.s^{-1}
γ	viscous damping constant, kg.s^{-1}
$\dot{\gamma}$	shear rate, s^{-1}
δ	particle overlap, m
ε_f	fluid volume fraction, dimensionless
ε_0	permittivity of free space, A^2.s^4.kg^{-1}.m^{-3}
ε	relative permittivity, dimensionless
κ	Debye screening length, m^{-1}
μ	dynamic viscosity, Pa.s
μ_0	yield viscosity, Pa.s
ν	Poisson's ratio, N.m^{-1}
ρ	density, kg.m^{-3}
τ	viscous stress tensor of fluid, kg.m^{-1}.s^{-2}
τ_0	yield stress, Pa
ψ	electric surface potential, V
ω	particle rotational velocity, m.s^{-1}

Subscripts

f	fluid phase
i	particle i
j	particle j
n	normal
p	particle phase
pf	particle-fluid interaction
r	rolling
t	tangential

INTRODUCTION

Particulate suspensions are found in a variety of industries, e.g. chemical, mining, food processing, and cosmetics. Flow properties, or rheology, of particulate suspensions are highly dependent on the properties of the particles suspended within the base fluid (e.g. size, shape and surface properties). This is particularly true as the particles become smaller in size, which means that non-contact forces between particles also become important. As a result, suspensions usually exhibit complex non-linear responses to changes in shear stress and shear rate, which makes their flow behaviour difficult to predict.

Rheological studies focus on experimental measurement using rheometers (Figure 1) to measure fluid properties under different shear stress or shear rate conditions. However, simulating the behaviour of individual particles in a fluid allows a priori prediction of fluid rheology, which can be validated with experimental data. Furthermore, being able to simulate the individual particles, allows for easier study of their behaviour and effect on the fluid. This is a feature lost with empirical models that focus on the macroscopic behaviour.

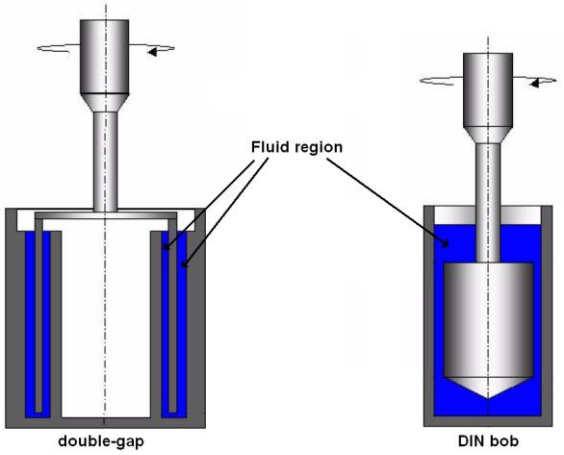

Figure 1: A cross-section of the double-gap and DIN bob rheometer geometries (TA Instruments, 2010)

A combination of Computational Fluid Dynamics (CFD) and Discrete Element Modelling (DEM) was used to model the particle-fluid system. CFD uses a continuum approach to model the fluid component, which is a fast and computationally efficient method. DEM on the other hand resolves the behaviour of each individual particle, and so accounts for the individual nature of the contact and non-contact forces between particles.

Because CFD and DEM are very different in their modelling approach, two separate software programmes were used. For CFD, OpenFOAM® (Weller et al, 1998) was chosen, and for the DEM, a programme called LIGGGHTS (Kloss and Goniva, 2010) was used. These two different codes could be coupled together with another programme called CFDEM (Goniva et al, 2010). CFDEM supports full four-way coupling where particle-fluid interactions, fluid-particle interactions, and particle-particle interactions are all considered. While four-way coupling is computationally more expensive than the more commonly used one or two-way coupling, it is necessary to handle all the important forces in a particulate system.

This paper describes the methodology used to develop a numerical model for the study of particulate suspensions. With this model, particle properties such as size, shape and surface charge can be studied to determine their overall effect on suspension rheology. The different models and equations used will be described, and some preliminary tests of the model will be presented.

CFD MODEL

The first phase was the development of a CFD model of a rheometer to test the performance of CFD against experimental data. Not only is it the fluid flow that drives the particle motion, but it is also the macroscopic behaviour of the fluid that is important in this investigation. For rheometers, it is assumed that the flow follows Couette flow, where the flow is also laminar and incompressible. In addition, the flow is also time-dependent due to the varying shear rate which occurs in controlled shear rate rheometers.

Model Description

A CFD mesh was created that mimicked the shape and behaviour of a rheometer. The simplest rheometer consists of one set of concentric cylinders. This is known as the single-gap rheometer. A double-gap rheometer is available and provides double the surface area for measurement. An adaptation of the single gap rheometer is the DIN bob, which has a conical tip to limit the influence of end effects (Figure 1).

In all cases, a thin slice of the full geometry was modelled, reducing the model size and computational expense. For the single and double gap, a horizontal slice was modelled as it was assumed the end effect would be negligible when compared to the full length of the rheometer. These geometries are axi-symmetric, which allowed them to be further reduced. The DIN bob geometry is more complex than the other two, but is axi-symmetric, which permits a thin 5° slice in the vertical direction.

CFD boundary conditions for the single-gap rheometer model are shown in Figure 2. These boundaries applied to all geometries. "No-slip" walls were used, with rotating wall boundaries given a tangential velocity corresponding to the required shear rate. In most cases, the shear rate was increased linearly over time. This allowed the model to replicate controlled-rate type rheometers. Slip at the rheometer walls was not considered in this study. Periodic boundary conditions were used on remaining boundaries.

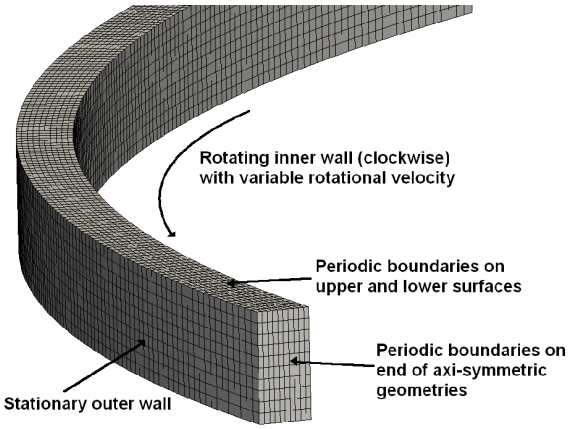

Figure 2: Geometry and boundary conditions for single-gap rheometer model

Torque on all rotating boundaries was calculated and converted to a shear stress value by multiplying it by a conversion factor. This factor depends on the type and dimensions of the rheometer geometry. A similar method was used for the shear rate. Equations describing these factors were taken from Whorlow (1992).

Newtonian Fluid Results

Water was selected as a benchmark fluid because most slurries contain water. The performance of the model was judged as to how close it could match the generally accepted value for water's dynamic viscosity at 20°C (1.004×10^{-3} Pa.s). OpenFOAM's "icoFoam" solver was used because the flow was assumed to be laminar, incompressible and unsteady.

Testing showed that the time step size did not significantly affect the results, although at larger time step sizes the model became unstable at higher shear rates. A time step value of 0.001s was found to be suitable for all cases. When axi-symmetric models were compared against much larger sections (90° and 360°), no significant difference was found. The smallest cell size used was 50μm.

The rate at which the shear rate changed over time was investigated. Figure 3 shows rheograms obtained from these models for the single-gap and DIN bob geometries. All simulations were run for maximum of 35s in real time. Modifications to rate of shear rate change were made for either the whole simulation time or for only the lower shear rates (<150 s^{-1}). The rate of shear rate change had the greatest effect at lower shear rates. Here, the faster the shear rate changed, the longer the values took to approach the final viscosity. A larger gap width (distance between the stationary and rotating wall) also increased the time it took for the viscosity to reach the final value, but the effect was not as significant as the change in shear rate. The large discrepancies between CFD and the experimental value at lower shear rates are thought to be as a result of the fluid being accelerated from rest relatively quickly. The mass of fluid takes a while to react to the acceleration of the rotating wall. Therefore a slower change in the shear rate is preferable as the correct viscosity is measured much sooner.

Another interesting finding was that at wider gap thickness (≥1mm), Taylor vortices were more likely to form within the gap at high shear rates. This follows experimental observations, which is encouraging from a qualitative point of view. These vortices are most likely the cause of the sharp increase in viscosity shown in both Figure 3A and B at higher shear rates (Barnes, 2000, Mezger, 2002).

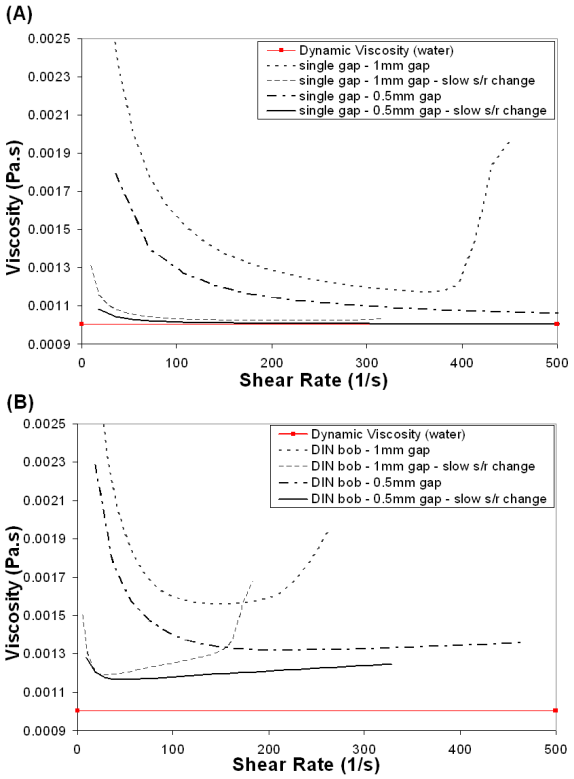

Figure 3: Results of the CFD model for a Newtonian fluid comparing different shear rate changes and gap widths for single-gap (A) and DIN bob (B) geometries

Both the single and double-gap geometries performed well at slower shear rate changes and smaller gap widths, with viscosity values within one percent of experimental viscosity. One important observation is the large difference between the performance of the DIN bob geometry and the other two. While both the single and double gap geometry are very accurate, the DIN bob does not even achieve a reasonable experimental error (10 – 50%). This is partly due end effects that are present in the DIN bob model (the ends of the single and double-gap models were not modelled).

Non-Newtonian Fluid Results

A non-Newtonian fluid was also tested as most suspensions are non-Newtonian. A mineral slurry containing a vermiculite-quartz mix was selected (Ndlovu et al, 2011). Herschel-Bulkley model parameters were fitted to the data. OpenFOAM's "nonNewtonainIcoFoam" solver was used.

Only the single-gap and DIN bob geometries were tested. Similarly with the Newtonian case, a good correlation was found between the fitted Herschel-Bulkley model and the CFD results. The DIN bob performed much better in this case, but still deviated slightly at higher shear rates. This shows the model was able to handle fluids that are more complex than simple Newtonian liquids.

DEM MODEL

A benefit of DEM is that it can provide dynamic information on individual particles in the system, such as particle trajectories and transient forces. In many cases this is extremely difficult, if not impossible, to obtain by physical experimentation. Consequently, DEM is being increasingly used to model discrete particle systems. The two types of particle motion, translational and rotational, are given by the following two equations respectively:

$$m_i \frac{dv_i}{dt} = F_{pf,i} + \sum_{j=1}^{z} \left(F_{c,ij} + F_{d,ij} \right) + m_i g$$

$$I_i \frac{d\omega_i}{dt} = \sum_{j=1}^{z} \left(M_{t,ij} + M_{r,ij} \right)$$

where z is the number of particles interacting with the particle. Forces involved are: the fluid-particle interaction (drag) force F_{pf}, the elastic collision force F_c, the viscous damping force F_d, and the gravitational force $m_i g$. The torques M_t and M_r represent the moments due to tangential forces and rolling friction torque respectively.

Particle-Particle and Particle-Wall Contact

LIGGGHTS uses the soft-sphere approach to modelling particle collisions. This approach, also developed by Cundall and Strack (1979), allows particles to deform or rather, overlap, during collisions which span multiple time steps. This overlap is used to calculate elastic, plastic and frictional forces between particles (Zhu et al, 2007). The main advantage of the soft-particle model is that lengthy collisions between several particles are allowed. Crucially, all inter-particle forces are accounted for during the collision. These are the two main considerations necessary for capturing the behaviour of dense suspensions (Hoomans et al, 1996; Apostolou and Hrymack, 2008). Unfortunately, very small time steps are required so that each collision can span multiple time steps, which increases the computational time of the simulation.

In an attempt to reduce computational effort, many DEM formulations use simplified models (and equations) to determine the forces and torques resulting from the contact

between particles. This is because complex models do not necessarily give more accurate results for the increase in computational expense (Zhu et al, 2007; Di Renzo and Di Maio, 2004). The most common linear model is the linear spring–dashpot model proposed by Cundall and Strack (1979), where the spring models the elastic deformation while the dashpot accounts for the viscous dissipation (Zhu et al, 2007).

LIGGGHTS has a number of different contact force models available. For computational efficiency reasons, the linear Hooke model was chosen. It uses a combination of a contact force and a damping force to calculate the force in both the normal (n) and tangential (t) directions. It is described as:

$$F = \left(k_n \delta n_{ij} - \gamma_n v n_{ij}\right) + \left(k_t \delta t_{ij} - \gamma_t v t_{ij}\right)$$

where k_n and k_t are elastic constants, γ_n and γ_t are viscoelastic damping constants, δn is the overlap distance of two particles, δt is the tangential displacement vector between two spherical particles (restricted to satisfy the Coulomb frictional limit, $F_t = \mu_c F_n$), and *vn* and *vt* are components of the relative velocity between particles. This contact model was used for particle-wall collisions as well.

DLVO Interaction Force

Many minerals have a natural surface charge due to their chemical structure (Ndlovu et al, 2011). DLVO forces were modelled to account for these non-contact attraction and repulsion forces between particles. The DLVO force, originally proposed by Derjaguin and Landau (1941) and Verwey and Overbeek (1948), is a combination of the van der Waals and electrostatic double layer forces.

LIGGGHTS includes two separate functions to simulate the van der Waals and electrostatic forces between the particles. Combining both these functions would result in the equivalent DLVO force. The van der Waals force was modelled with a modified "colloid" function, which uses the following relation to calculate the interaction energy:

$$E_{vdw} = -\frac{A_H}{6}\left[\frac{2r_i r_j}{r^2-\left(r_i+r_j\right)^2} + \frac{2r_i r_j}{r^2-\left(r_i-r_j\right)^2} + \ln\frac{r^2-\left(r_i+r_j\right)^2}{r^2-\left(r_i-r_j\right)^2}\right]$$

The electrostatic (electric double layer) interaction is simulated by a modified "yukawa/colloid" function:

$$E_{edl} = 2\pi\, r_i \varepsilon\varepsilon_0 \psi^2 e^{-\kappa(r-(r_i+r_j))} \qquad r < r_c$$

where r is the separation distance between particle centres, r_i and r_j are the radii of the two particles, and ψ is equivalent to the zeta potential (ζ). Both functions are only active for separation distances below the cut-off distance (r_c). A longer cut-off distance reduces computational efficiency as the force influences more particles. Particles are allowed to overlap each other during collisions, which could cause these functions to become invalid. Therefore a minimum separation distance limit was added so the magnitude of the force did not become undefined during the collision.

Fluid-Particle Drag Force

The drag force is the means by which the fluid imparts motion onto the particles. In dense systems, like that found in a rheometer, the presence of surrounding particles will affect the drag force, and so a more complex formulation is needed. There are two commonly used drag models for particle-fluid systems. The older, more established, model by Ergun (1952) and Wen and Yu (1966) is often used, but introduces a discontinuity at a particle volume fraction of 0.2. Di Felice's correlation (1994) closely approximates that of Ergun, Wen and Yu, but eliminates the discontinuity, providing a much smoother change in drag force. Therefore Di Felice's drag model was employed here. This model, available in CFDEM, is given by:

$$F_{pf}(\varepsilon_f) = 0.5 c_{do} \rho_f \pi\, r_i^2 \left|u - v_i\right| (u - v_i) \varepsilon_f^{-(\alpha+1)}$$

where: $\alpha = 3.7 - 0.65\exp\left[\frac{-(1.5-\log_{10}\mathrm{Re}_p)^2}{2}\right]$

COUPLED CFD-DEM MODEL

A number of practical factors had to be considered for the design of the coupled model. In particular, it was expected to use this model to simulate particle systems of high particle volume fraction (up to 0.6). Also, the smallest particle that was considered was 1.5 μm in diameter. In the geometries tested with the CFD model, this would have led to an excessive amount of particles in the domain, with exorbitant computational costs. Therefore the model design and size had to be reduced to mitigate this problem.

Governing Equations for Coupled Flow

The fluid phase equations have to be altered to include the effects of momentum transfer due to particles suspended within the fluid. Most literature regarding fluid-particle systems mentions two different formulations of the fluid flow equations that are commonly used, namely Model A and Model B (Zhu et al, 2007; Feng and Yu, 2003). Zhou et al (2010), however, proposes that there are actually three formulations and discusses the applicability of each one to different systems. Based on their analysis, Model A would be more suitable for this system. This is because Model B is only valid when the fluid flow is steady and uniform or when the residual force on the particles is zero. These conditions are not strictly true for this type of system.

Model A is described by the following two equations, where the first equation describes conservation of mass, and the second describes conservation of momentum:

$$\frac{\partial\left(\varepsilon_f\right)}{\partial t} + \nabla\cdot\left(\varepsilon_f u\right) = 0$$

$$\frac{\partial\left(\rho_f \varepsilon_f u_f\right)}{\partial t} + \nabla\cdot\left(\rho_f \varepsilon_f u_f u_f\right) = -\varepsilon_f \nabla p - F_{pf} + \varepsilon_f \nabla\cdot\tau + \rho_f \varepsilon_f g$$

where F_{pf} is the volumetric particle-fluid interaction force. This force is made up of the particle drag force, the pressure gradient force, and the viscous force due to fluid shear stress.

Coupled Model Geometry and Boundary Conditions

In order to take advantage of LIGGGHTS' limited ability to handle periodic boundaries, the circular CFD domains were restructured into a flat-edged box. This is equivalent to unravelling the circular ring of the single-gap rheometer into a linear domain with one wall translating past the other. To further reduce the number of particles required, a smaller domain size was also used. A smaller model is quicker to solve, but may lose its value as a representative sample. The lower limit of the box size is still under investigation, but the current size is a cube with sides of 50 µm in length. For 1.5 µm diameter particles this results in just over 35 000 particles at a volume fraction of 0.5.

Even with the new domain shape, the boundary conditions remain the same (Figure 4). There are two walls, one stationary outer wall, and a (now) translating inner wall mimicking the rotational movement of the cylindrical surface in a conventional rheometer. Periodic boundaries extend the flow in the vertical and horizontal directions.

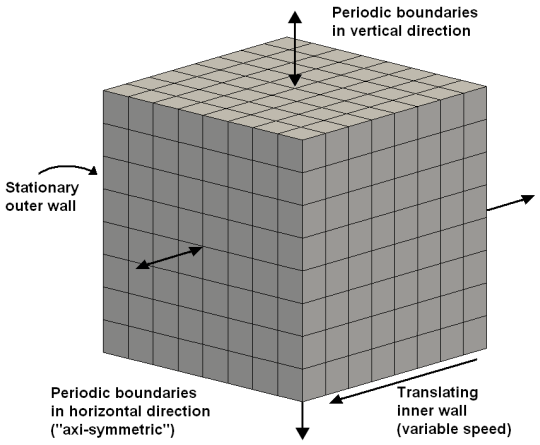

Figure 4: Boundary conditions for coupled model

According to preliminary CFD tests (water only), the values generated by the box geometries are just as accurate as the cylindrical single-gap rheometer geometries (up to six percent), but underestimate the experimental viscosity value instead of overestimating it like the circular geometries. This might be explained by flat edges of the box versus the curved rheometer geometries. Different box dimensions, did not affect the results significantly as the different sizes achieved errors within two percent of the experimental value. Increasing the gap width to 500 µm had the most effect, increasing the error to six percent.

In addition, the box geometries were found to be mesh-independent, with cell sizes ranging from 3 to 12 µm (along each side). This is to be expected for such a simple flow geometry.

Time Step Size and Coupling Procedure

Due to the physics involved in many coupled systems, the DEM time step generally needs to be much smaller than the CFD time step. The time step has to be sufficiently small to capture the energy transmission by wave propagation (Li, Xu and Thornton, 2005). To establish the upper limit of the DEM time step, the criteria of the Rayleigh time was used, as it is typically suited to dense systems. Rayleigh time is the time taken by the Rayleigh surface wave to propagate through a solid particle. It is good practice to select the time step as a fraction of the Rayleigh time, typically in the region of 0.1 – 0.3. Rayleigh time is defined as:

$$dt_R = \frac{\pi\, r \sqrt{\rho_p / G}}{(0.1631\nu + 0.8766)}$$

CFDEM runs the CFD and DEM solvers concurrently. Because the CFD timestep is often much larger than the DEM timestep, the DEM solver runs for a number of timesteps before the information is transferred to the CFD solver, which usually only iterates for one timestep between coupling. The coupling interval is typically in the region of 50 – 100 timesteps.

Preliminary Validation of Coupled Model

In order to validate the coupled model, experimental data from Megias-Alguacil, Duran and Delgado (2000) was used. Part of their work covers rheological data for spherical zirconia particles. They also include detailed data on the DLVO interaction forces which is useful in reconstructing the material parameters needed in the computer model. However, all simulations have not been completed yet, and so only preliminary results are presented here (Figure 5).

Material parameters for zirconia particles result in a DEM timestep size of $1x10^{-9}$ seconds, as recommended by the Rayleigh criteria. This was due largely to the small particle size modelled (1.5 µm). Selecting a larger coupling interval of 100, gives a CFD timestep size of $1x10^{-7}$ seconds. Shear rates were increased linearly from zero, up to 180 s^{-1}.

CFD mesh cell size was selected based on particle diameter. A cell with edge length of 4.2 particle diameters (6.25 µm) was sufficiently large for the assumption of unresolved CFD-DEM coupling. This results in a mesh of 512 cells. Bigger cells of 5.6 particle diameters in length were tested, but were found to give different results.

Figure 5 compares initial coupled model results with the experimental values for a particle volume fraction of 4.68% and pH of 4.5 (with a corresponding zeta potential of 32 mV). CFD results for pure water are also shown for comparison to illustrate the effect of adding particles to the model. For the coupled model, the torque value used to calculate the shear stress is a combination of the fluid viscous force on the translating boundary and the tangential force due to particles impacting that same surface. As can be seen from Figure 5, plain particles (no DLVO forces) significantly increase the shear stress. Including DLVO forces further increases the overall shear stress as expected. However, it did not produce a sizeable increase in shear stress as the shear rate was increased, which was expected from the experimental data trend. This might be a result of a mesh that is too coarse, where the particle effects are diffused into the general flow.

Pure fluid flow in a box is simple enough to be mesh independent, but adding particles increases flow complexity. Furthermore, distribution of particles into their respective CFD cells during the coupling procedure changes with different meshes. These factors indicate that the coupled model would not be as mesh independent as the pure fluid simulations.

It should be noted that the experimental data were measured using a coaxial cylinder geometry, whereas the numerical results were calculated for a box-shaped

domain. However, box and single-dap geometries were found to be equivalent (produce similar results) in pure CFD tests.

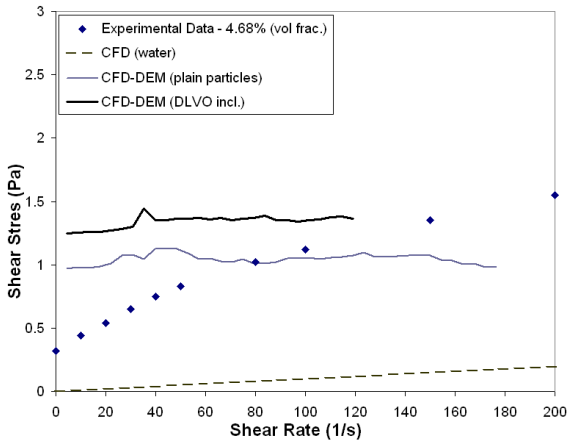

Figure 5: Rheogram comparing preliminary coupled model results with experimental values

Simulations were conducted on a high performance cluster, consisting of 2.93 GHz Intel processors, with 8 cores on each node. Memory for each node was 12 GB, though the coupled simulations typically only required 1 – 2 GB. Particle-fluid systems (including DLVO forces) took around 10 days to compute with 8 CPU cores. Removing DLVO forces halved the computational time.

CONCLUSIONS

The methodology for the development of a CFD-DEM numerical model for particulate suspensions has been described. At each major step in the development, testing has been done to assess its behaviour under different conditions. For the pure CFD model, the results were very good. Accurate representations of the known fluid material behaviour for both Newtonian and non-Newtonian cases were achieved. In addition, the results show that slower changes in shear rate, and gap widths of less than 1mm produce more accurate results over a larger shear rate range.

Preliminary behaviour of the coupled model is reasonable and follows some good trends. However, work still needs to be done to refine it further. In particular, the coupling interval and mesh size still need to be fully explored. Once the development and validation of the model has been completed, it will provide interesting insights into the rheology of particulate suspensions. Preliminary tests show the model to be fast and efficient, but the number of timesteps that are required results in long computational times.

REFERENCES

APOSTOLOU, K. and HRYMACK, A.N., (2008), "Discrete element simulation of liquid-particle flows", *Computers and Chemical Engineering*, **32**, 841-856.

BARNES, H.A., (2000), *Handbook of Rheology*, 45 p, University of Wales, Aberystwyth.

CUNDALL, P.A. and STRACK, O.D.L., (1979). "A discrete numerical model for granular assemblies", *Geotechnique*, **29**, 47–65.

DERJAGUIN, B.V and LANDAU, L., (1941), "Theory of the stability of strongly charged lyophobic sols and of the adhesion of strongly charged particles in solutions of electrolytes", *Acta Physicochem*, **14**, 633–662.

DI FELICE, R., (1994), "The voidage function for fluid–particle interaction systems", *Int. J. of Multiphase Flow*, **20**, 153–159.

DI RENZO, A. and DI MAIO, F.P., (2004), "Comparison of contact-force models for the simulation of collisions in DEM-based granular flow codes", *Chemical Engineering Science*, **59**, 525-541.

Ergun, S., (1952), "Fluid flow through packed columns", *Chemical Engineering Progress*, **48**, 89–94.

FENG, Y. and YU, A., (2003), "Numerical simulation of the gas-solid flow in a fluidized bed by combining discrete particle method with computational fluid dynamics", *Third Int. Conf. on CFD in the Minerals and Process Industries*, Melbourne, Australia, December 10-12.

GONIVA, C., KLOSS, C., HAGER, A. and PIRKER, S., (2010), "An Open Source CFD-DEM Perspective", *Proc. of OpenFOAM Workshop*, Göteborg, Sweden.

HOOMANS, B.P.B., KUIPERS, J.A.M., BRIELS, W.J. and VAN SWAAIJ, W.P.M., (2006), "Discrete particle simulation of bubble and slug formation in a two-dimensional gas-fluidised bed: a hard-sphere approach", *Chemical Engineering Science*, **51**, 91-111.

KLOSS, C. and GONIVA, C., (2010), "LIGGGHTS – A New Open Source Dem Simulation Software", *5th Int. Conf. on Discrete Element Methods (DEM5)*, London.

LI, Y., XU, Y. and THORNTON, C., (2005), "A comparison of discrete element simulations and experiments for 'sandpiles' composed of spherical particles", *Powder Technology*, **160**, 219-228.

MEGIAS-ALGUACIL, D., DURAN, J.D.G. and DELGADO, A.V., (2000), "Yield stress of concentrated zirconia suspensions: correlation with particle interactions", *J. of Colloid and Interface Science*, **231**, 74-83.

MEZGER, T.G., (2002), *The Rheology Handbook*, pp 33-34, Vincentz Verlag, Hannover.

NDLOVU, B., BECKER, M., FORBES, E., DEGLON, D. and FRANZIDIS, J.P., (2011), "The influence of phyllosilicate mineralogy on the rheology of mineral suspensions", *Minerals Engineering*, **24**, 1314-1322.

TA INSTRUMENTS, 2010, AR-G2 Rheometer operator's manual.

VERWEY, E.J.W., and OVERBEEK, J.T.G., (1948), Theory of the stability of lyophobic colloids - The interaction of soil particle having an electrical double layer, Elsevier, Amsterdam.

WELLER, H.G., TABOR, G., JASAK, H., and FUREBY, C., (1998), "A tensorial approach to computational continuum mechanics using object orientated techniques", *Computers in Physics*, **12**, 620–631.

WEN, Y.C. and YU, Y.H., (1966). "Mechanics of Fluidization", *Chemical Engineering Progress Symposium Series*, **62**, 100–111.

WHORLOW, R.W., (1992), *Rheological techniques*, 2nd edition, Ellis Horwood.

ZHOU, Z.Y., KUANG, S.B., CHU, K.W. and YU, A.B., (2010), "Discrete particle simulation of particle-fluid flow: model formulations and their applicability", *J. of Fluid Mechanics*, **661**, 482-510.

ZHU, H.P., ZHOU, Z.Y., YANG, R.Y. and YU, A.B., (2007), "Discrete particle simulation of particulate

systems: theoretical developments", *Chemical Engineering Science*, **62**, 3378-3396.

